Proceedings of the ASME 2020 15th International Manufacturing Science and Engineering Conference MSEC2020 September 3, 2020, Virtual, Online

MSEC2020-8378

EMBEDDED SENSING CAPABILITIES IN AN FDM PRINTED OBJECT

Garrett McGrady, Neel Jain, Douglas Jackson University of Louisville Louisville, KY Kevin Walsh University of Louisville Louisville, KY

ABSTRACT

The objective of this paper is to demonstrate the flexure properties of ABS plastic in a 3D printed object as a process to enable embedded pressure sensing capabilities. Developing the potential for non-static 3D parts broadens the scope of the fused deposition modeling (FDM) process to include printing 'smart' objects that utilize intrinsic material properties to act as microphones, load sensors, accelerometers, etc. In order to demonstrate a strain-based pressure transducer, strain gauges were embedded either directly on top or in the middle of a flexible ABS diaphragm.

Securing a strain gage directly on top of the diaphragm traced a reference pressure more closely than diaphragms with the strain gage embedded halfway into the diaphragm. To prevent temperature-related drift, an additional strain gage was suspended above the secured gage, inside the 3D printed cavity. The additional gage allowed for a half-bridge circuit in lieu of a quarter-bridge circuit, which minimized drift due to temperature change. The ABS diaphragm showed no significant signs of elastic hysteresis or nonlinear buckling. When sealed with 100% acetone, the diaphragm leaked ~50x slower than as-printed sensors. After pressurizing and depressurizing the devices multiple times, they output pressure readouts that were consistent and repeatable for any given pressure within the operational range of 0 to 7psi.

The repeatability of each of the final generation sensors indicates that 'smart' objects printed using an FDM process could be individually calibrated to make repeatable recordings. This work demonstrates a concept overlooked previous to now—FDM printed objects are not limited to static models, which lack dynamic motion of the part as an element of design. Altering FDM's bottom-up process can allow for easily embedding sensing elements that result in printed objects which are functional on the mesoscale.

1. INTRODUCTION

Fused deposition modeling (FDM) is a rapid prototyping method that prints objects bottom to top in layers of a plastic material – often Acrylonitrile-Butadiene-Styrene (ABS) [1, 2]. FDM prints are generally static models with no dynamic application. Static models may be used functionally as a load-bearing part; however, they have no integration of sensing elements to exploit the flexure properties of the part's material.

A perceived drawback of FDM printed parts is structural inhomogeneity [3]. FDM printers, due to the limitations of their extruder size, are used to print objects on the mesoscale (>1mm x 1mm). Skepticism surrounding FDM has propelled expectations into an economic trough of disillusionment [4]. However, by utilizing the material properties of ABS, FDM printed parts have the potential to become 'smart' objects with sensing capabilities. This work focuses on the optimal design of a pressure sensor to further the conversation of 3D printed intelligent objects. The primary purpose for conducting this work is to demonstrate that the FDM process flow can be modified and the flexure properties of ABS can be exploited in such a way that sensing capabilities can be embedded in parts to make them 'smart.'

Currently, the state-of-the-art for creating 'smart' parts involves aerosol jetting conductive inks onto 3D-printed plastic parts [5]; however, aerosol jetting systems are prohibitively expensive, and no process exists for in-situ aerosol jetting conductive ink during the FDM process. Printers such as the Voxel8 have attempted to integrate conductive inks with FDM [6]; however, its feature size is too large to accommodate directly printing optimal strain gage geometries [7], and it is typically used in antenna-based applications [6]. Additionally, the silver inks used by either the Voxel8 or an aerosol jetting system are relatively expensive and are subject to a shelf life.

As a goal, it was pre-determined that factors qualifying a design as 'optimal' would be a pressure sensor which integrates a pre-made strain gage, exhibits limited leak rate, limited

hysteresis, and limited drift. Additional outcomes of an optimal sensor design would be maximal sensitivity to changes in pressure and repeatability of pressure readouts. This research represents a model that may apply on multiple scales; however, at the micro- and nanoscales, nonlinear buckling—not observed on the mesoscale—of diaphragms similar to the one presented here are difficult to model.

2. MATERIALS AND METHODS

2.1 Sensor Structure

A Zortrax M200 3D printer was used to fabricate the FDMprinted pressure sensor case study. The M200 system has a resolution of 80-400um with a nozzle diameter of 400um [8]. The large range in resolution is to allow for fine features and precise dimensioning of modeled parts. An ABS plastic filament was chosen for the sensor material due to its common use, strength, and cost effectiveness [1, 9]. The print recipe for all parts was a layer height of 0.19mm and a print speed of 100mm/s. Parts were printed with no support structures, and the infill was set to "high" in the proprietary Z-Suite slicing software. As shown in Figure 1, the overall design of the pressure sensor consisted of a small cubic-like object containing a hollow conical interior cavity, thin circular diaphragm, side vent port to the exterior, and small "micro-channels" for electrical wiring. This design was chosen since the conical cavity requires no vertical support structures to print and the circular diaphragm at the base of the cavity has an understood behavior when exposed to pressure (see Section 2.4).

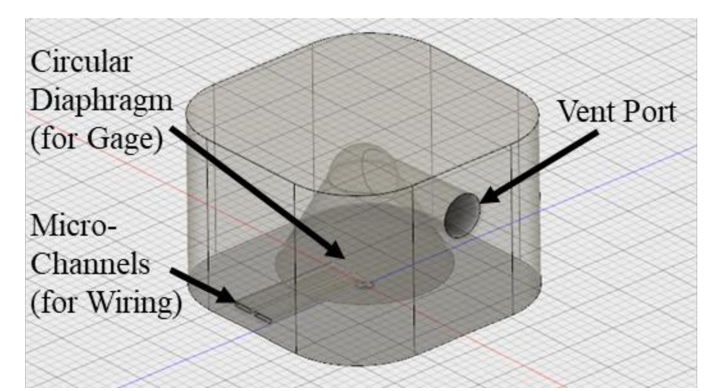


FIGURE 1: ISOMETRIC VIEW OF SENSOR STRUCTURE

To function as an integrated pressure sensor, a strain gage was strategically incorporated into the sensor design either on or embedded inside the thin circular diaphragm. Running from the chamber on the left side of the sensor structure are two extrusions or micro-channels which were used to guide the wires of the strain gage to the exterior. The bottom surface of the conical chamber essentially defined the lateral dimensions of the thin circular diaphragm, which was 18mm in diameter for all sensors. In total, five variations of the sensor design were considered (see Table 1). A test for sensitivity was implemented on each of the five designs, all of which had either a 1mm or 2mm thick diaphragm.

TABLE 1: VARIATIONS OF AN EMBEDDED GAGE TO DETERMINE OPTIMAL DEPTH STRAIN INTEGRATION

Diaphragm Thickness	Depth of Embedded Strain Gage
1.0 mm	0.0 mm (interior surface)
1.0 mm	0.5 mm
2.0 mm	0.0 mm (interior surface)
2.0 mm	0.5 mm
2.0 mm	1.0 mm

2.2 Diaphragm Sealing

Two main methods were tested on ABS diaphragms to assess sealing effectiveness—parylene coating and acetone treatment. In parylene coating, the target thickness was 50 um, which was achieved by vaporizing 15g of parylene C. Acetone treatment consisted of repeatedly dipping the diaphragm of a sensor part in 100% Acetone at a rate of 1cycle/sec for either 10, 20, or 30 seconds. Three methods were tested to determine the most effective form of acetone sealing—repeated dipping at a set frequency, full immersion, and cold vapor bath.

Sealed 18mm diaphragms were tested by pressurizing them to 5psi using a reference pressure sensor attached to the source tank. The tank valve was opened to allow air to flow into the part, pressurizing it. Then, using a stopwatch, the time it took the part to leak from 5 to 4psi was recorded in seconds. For the purpose of process comparison, a minimal leak rate can also be defined as a maximum time to leak from 5 to 4psi.

2.3 Embedding Single & Multiple Gages

During the 3D printing process, a tool head pause was added at the depth where the strain gage was to be embedded and a two-part epoxy was used to secure the strain gage to the diaphragm. After 5 minutes, the epoxy had set, and tweezers were used to manipulate the wires from the gage to run out the side extrusions, which were exposed during the pause. Figure 2 shows an example of a single gage being secured to the diaphragm.

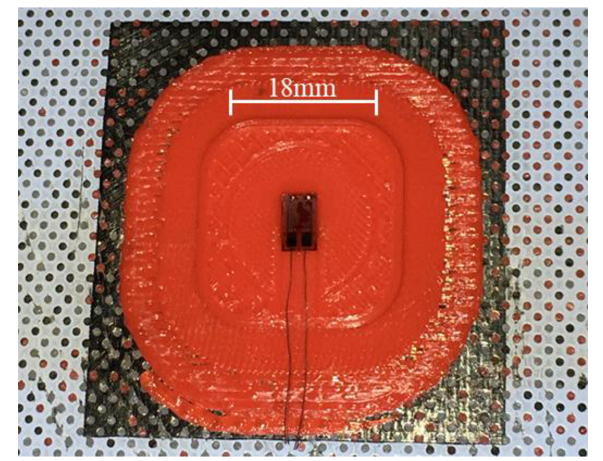


FIGURE 2: A GAGE SECURED IN THE CENTER OF THE 18MM DIAPHRAGM

Once the gage was fixed and its wires fed through the partially created micro-channels, the print was resumed. Depending on whether the gage was embedded within the diaphragm or simply fixed on top of it, the printer's extruder either continued printing layers directly over the strain gage or began forming the sides of the conical cavity, respectively.

Anticipating that a single gage, quarter-bridge circuit might not fare well against thermal drift, a second generation of the sensor was designed so that a dummy gage could be placed in the conical cavity, suspended inside of it. Figure 3 shows this technique during a pause in the print.

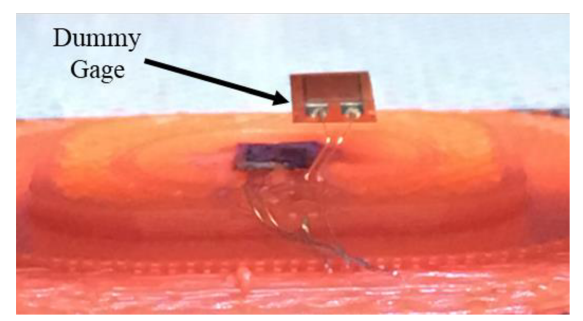


FIGURE 3: A DUAL GAGE SENSOR DESIGN APPROPRIATE FOR HALF-BRIDGE OPERATION

The structural design of the sensor housing was not changed; however, during the pause, after fixing one strain gage to the diaphragm and running both of its wires out of one side extrusion, another gage was placed next to it and its wires were secured with epoxy along the second side extrusion. During this process, it was important to consider the vertical position of the suspended dummy gage as it can interfere with the decreasing radius of the conical cavity. Care was taken to ensure that as the printer resumed printing, the extruder nozzle would not come into contact with the suspended gage; therefore, the dummy gage was suspended as close above the first gage as possible without allowing them to make physical contact.

The addition of a second gage allowed for operating the sensor in a half-bridge configuration, which was predicted to be inherently less sensitive to thermal drift. In the single gage quarter-bridge design, the output of the sensor is dependent on changes in the one gage's resistance, which is dependent on both pressure and temperature [10]. In contrast, the dual-gage half-bridge design has an output which is dependent on changes in the ratio of the two gages' resistances, and any common-mode changes, such as that due to temperature, should be filtered out.

2.4 Sensitivity Testing

In testing for sensitivity, there were two design choices to be made: optimal diaphragm thickness and optimal depth of strain gage embedding. Optimal diaphragm thickness was chosen based on the deformation of 1mm vs. 2mm diaphragms from 0 to 10psi. In theory, the deformation of the center point on a circular diaphragm is dependent on the behavior of its edges [11]—whether they are simply supported or fixed. Equations 1 and 2 govern the magnitude of center point deflection y_o for simply supported and fixed edges, respectively:

$$y_0 = \frac{3}{16}(1 - v^2) \frac{5 + v}{1 + v} \left(\frac{Pa^4}{Eh^3}\right) \tag{1}$$

$$y_0 = \frac{3}{16}(1 - v^2) \left(\frac{Pa^4}{Eh^3}\right) \tag{2}$$

where v is the Poisson ratio of ABS, P is applied pressure, a is diaphragm radius, h is the diaphragm thickness, and E is an experimental Young's Modulus. Using a material test system, the Young's Modulus of 1mm and 2mm printed ABS samples, which were treated with 100% acetone, was found to be 1.78 and 1.17 GPa, respectively. The fixed edge and simply supported models represent extremes for deformation due to pressure.

Unfortunately, the edge behavior of FDM printed diaphragms has not been well characterized. Given that the simply supported and fixed edge models represent extremes of edge behavior, it was our hypothesis that the ABS diaphragm would have a deformation pattern somewhere between those two extremes. Using the assumption that the 100% acetone treatment created a uniform stress throughout the thickness of the diaphragm (see Equation 3), Equation 4 was derived as an intrinsic stress model of deformation to predict the treated ABS diaphragms' center point deformation:

$$\sigma_i = \frac{2zEh}{L} \tag{3}$$

$$y_0 = \frac{Pa^2}{4\sigma_i h} \tag{4}$$

where L is the length of a printed sample beam and z is the vertical deflection of the curled beam after it has been treated on one side with acetone. All three models for center point deflection assume a linear relation between input pressure P and center point deflection y_o . The sensors were pressurized to 10psi to test the validity of the intrinsic stress model.

2.5 Embedded Strain Gage Depth

Depth of the embedded strain gage was also optimized by examining each sensors' response to a repetitive pressure sweep. Each of the five sensors tested (see Table 1) was constructed with a single embedded gage, which allowed for a quarter-bridge circuit on a P3 Strain Gage Indicator and Recorder. The P3 Strain Gage Indicator and Recorder is a device that accepts input from the embedded strain gages, amplifies the bridge, and outputs static strain of the system [12]. An analog output setting on the P3 Indicator (0-2.5V) was used to track the value of strain from each quarter-bridge in LabVIEW. The P3 Indicator was calibrated with a LOW pass setting, such that -320uE to 320uE corresponds to a 0V to 2.5V analog output and -10psi to 10psi experimental sensor pressure. A LabVIEW program and a reference pressure sensor were employed to perform a pressure sweep from 0psi to 5psi and a subsequent depression from 5psi to -5psi. The reference pressure sensor was connected along the same line of pressure as the experimental sensor. The reference

pressure sensor output a voltage, which corresponds to its measured pressure—this variable is referred to in the results as reference voltage or reference pressure, which ranges from -2.5V to 2.5V and represents -10psi to 10psi. Analyzing the reference pressure in comparison to the back-calculated analog strain readout from the experimental sensor circuit revealed the sensitivity of the diaphragms under stress.

3. RESULTS AND DISCUSSION

3.1 Diaphragm Sealing

In Table 2, qualitative ratings of effectiveness were assigned based on the time to leak from 5psi to 4psi. Excellent corresponds to >10min, an acceptable rating corresponds to 5-10min, and an ineffective rating corresponds to <1min leak time. The goal of achieving an 'optimal' sensor would maximize time to leak, since leak rate is inversely related to the time it takes a sensor to leak 1psi.

TABLE 2: DIAPHRAGM SEALING WITH 100% ACETONE

Method	Effectiveness	Effect on Part
Dipped; 30 cycles; 1	Excellent	Sealed
cycle/sec		
Dipped; 20 cycles; 1	Acceptable	Sealed
cycle/sec		
Dipped; 10 cycles; 1	Acceptable	Sealed
cycle/sec		
Full Immersion	Ineffective	ABS Expansion &
		Deformation
Cold Vapor Bath	Ineffective	Unequal Coating

The number of cycles for the repeated dipping was varied to determine which amount of time proved most effective. Although all variations of repeated dipping yielded a significant seal when compared to the as-printed parts, at 30 cycles, the diaphragm is most effectively sealed. Higher cycle counts were not tested since parts began to show signs of ABS dissolution at \sim 35 cycles.

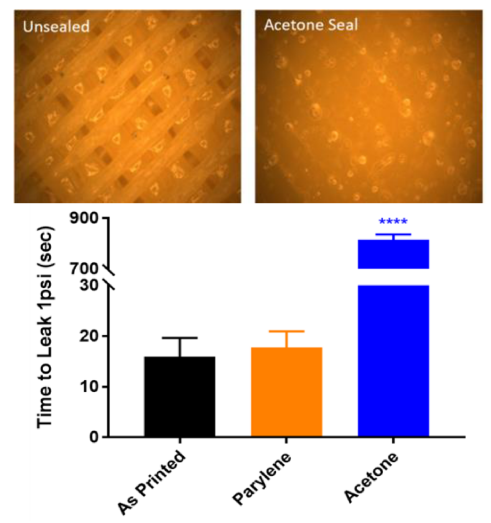


FIGURE 4: ACETONE SEALING INCREASES LEAK TIME

Five sensors were sealed using each method—parylene coating and the most effective acetone treatment identified above. Figure 4 shows that after being coated with parylene, the sensors still showed no significant difference in leak time as compared with the unsealed controls. It should also be noted that the parylene coating, while the target thickness was 50um, varied across the diaphragm and part anywhere from ~30um to ~120um. Coatings on the side walls of the ABS part were generally thicker than the coating across the diaphragm itself. The acetone treatment yielded diaphragms that leaked ~50x slower than the controls, where the average time to leak 1psi was recorded at 815sec. An unpaired t-test of the acetone-treated sensors compared to the control data returned a p-value of <0.0001. Therefore, the acetone dipping treatment at 1cycle/sec for 30 cycles was determined to be an effective sealing method.

3.2 Sensitivity Testing

Figure 5 shows the deformation test for 1mm and 2mm diaphragms. The original hypothesis was supported—the intrinsic stress model closely resembles the experimentally obtained pressure readings. Pressurizing 1mm and 2mm diaphragms over a constant domain of pressures showed that 1mm diaphragms operate over a larger range of outputs, indicating that they enable higher precision than 2mm diaphragms. The center-point deformation of those 1mm diaphragms is linearly related to applied pressure up to ~7 psi.

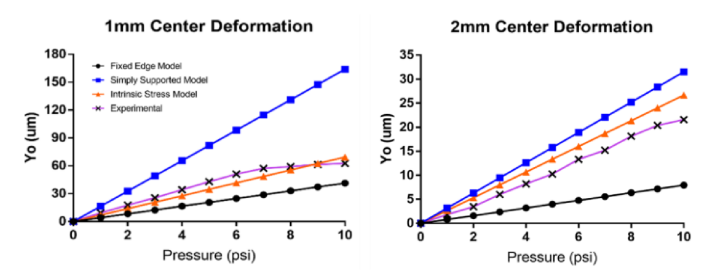


FIGURE 5: THREE MODELS OF EDGE BEHAVIOR WITH EXPERIMENTAL RESULTS

3.3 Optimal Embedded Gage Depth

Figure 6 presents results for the sensitivity test—one that involved single-gage, 1mm thick diaphragm sensors during a pressurization from 0psi to 5psi and a subsequent vacuum from 5psi to -5psi. Reference voltage is the output of a reference pressure sensor connected in parallel on the pressure line to the experimental sensor. Sensor strain is the back-calculated value of strain from the analog output of the P3 Indicator, and it corresponds to pressure observed in the experimental sensor under test. Figure 6a shows the pressure sweep data for a 1mm diaphragm with the strain gage placed directly on top of the diaphragm, and 6b shows the data for a 1mm diaphragm with the strain gage embedded within the diaphragm at a depth of 0.5mm.

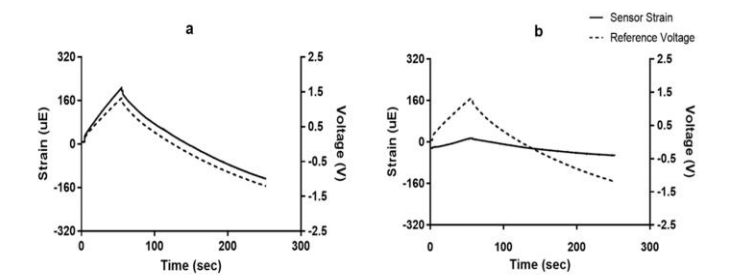


FIGURE 6: SENSITIVITY EFFECT OF EMBEDDING THE STRAIN GAGE

The experimental voltage trend for the sensor design in which the strain gage is placed directly on top of the diaphragm (Figure 6a) follows the reference voltage well. The sensor strain for the gage embedded within the diaphragm (Figure 6b) does not follow the reference voltage, which may be due to the strain gage being closer to the neutral axis of the deflection. When analyzing each sensors' response to a pressure sweep, the inversely proportionate ratio of absolute change in experimental strain versus reference voltage that was observed when the strain gage was placed on top of the diaphragm indicates that it is more sensitive to tensile and compressive forces along the full duration of the pressure sweep.

3.4 Drift due to Temperature

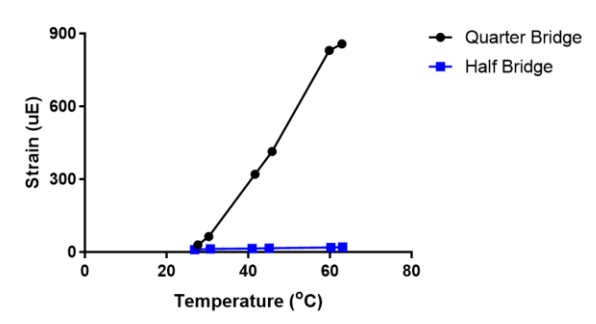


FIGURE 7: DRIFT DUE TO TEMPERATURE OF HALF AND QUARTER BRIDGE CIRCUIT DESIGNS

After identifying the design best suited for sensing capabilities (1mm diaphragm w/ a strain gage secured directly on top of the diaphragm), it was imperative to test both quarter-and half-bridge sensor-types for drift due to temperature fluctuation. A 1mm diaphragm sensor with diameter of 18mm was printed with dual strain gages. The dual gages design allows for the same sensor to be tested with either a quarter- or half-bridge configuration on the P3 Indicator; thus, the data in Figure 7 is from one sensor part. When hooked up as a quarter-bridge circuit, the sensor's output is sensitive to temperature change, drifting to 858uE, which back-calculates to an inaccurate apparent ~26.8psi. The range of the quarter-bridge strain is ~820uE, whereas the range of the half-bridge data is 10uE. The half-bridge drifts to only 21uE, or an apparent pressure of ~0.26psi. Therefore, in a reasonable operating range of

temperatures, the quarter-bridge device is highly sensitive to temperature change, and the half-bridge device is resistant to temperature fluctuation, as was expected. Any deviation from the accurate pressure in half-bridge circuits could be reasonably eliminated during calibration of the device since the error is relatively constant.

3.5 Repeatability

Three sealed, half-bridge sensors were pressurized to 5psi and subsequently vacuumed down to 0psi ten times in succession to test the repeatability of each sensor. The three sensors had 1mm diaphragms with dual gages embedded directly on top of the interior surface, and the diaphragm was sealed with acetone. Figure 8 shows the results of one sensor's ten "runs" of being pressurized to 5psi and vacuumed to 0psi.

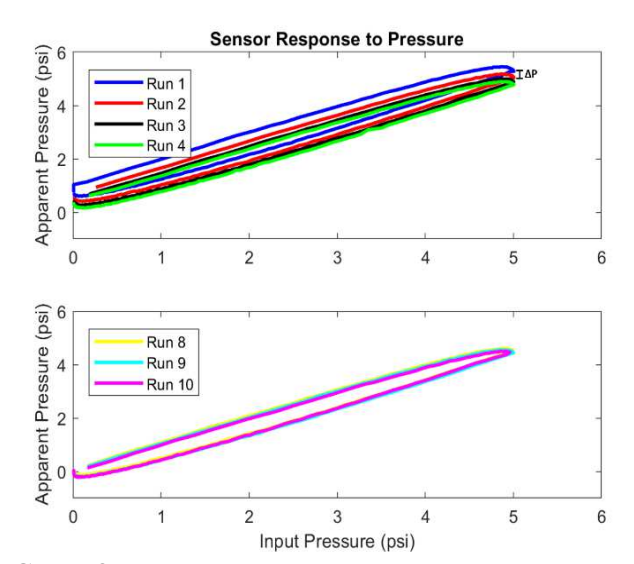


FIGURE 8: REPEATABILITY OF FINAL SENSOR DESIGN

In each run, there is an observed hysteresis on the return path to 0psi; however, this hysteresis does not appear to affect the repeatability of the sensor after several runs. The drift of the sensor from run to run, noted in Figure 8 as ΔP , approaches zero as the sensor experiences ~8 runs. Six iterations of the sensor showed similar results to those presented in Figure 8. Each sensor operated in its own range of apparent pressures. This discrepancy from part to part was expected as a symptom of FDM printing; however, each sensor is precise to itself, which would allow for individual calibration of each part.

The discrepancies between sensors is likely due to variance in the human interaction with the process. For example, the two-part epoxy applied on the surface of the diaphragm may not be the same amount each time. Furthermore, the thickness of the epoxy likely has an effect on the readout of the strain gage; thus, if not controlled, the epoxy could be a source of discrepancy. Process variables that affect the cure of the epoxy such as the temperature of the diaphragm at time of application and the cure status of the epoxy when the gage is placed could affect how each

gage experiences strain in response to pressure. Finally, the acetone sealing process may also create slight differences between sensors as it seals the diaphragm. The acetone sealing process is completed by a human; thus, there is likely variance in the sealing process. Such variance could affect the intrinsic stress of the diaphragms and their responses to pressure.

4. CONCLUSION

The engineering goal of this work was to fabricate a sensor that is sensitive, experiences minimal hysteresis and drift, is effectively sealed, and makes repeatable readings—a goal which was successfully met and supported by analysis of the data presented. The final sensor design included a 1mm diaphragm with two strain gages arranged into a half-bridge circuit and the diaphragm sealed with acetone to minimize leak rate. The sensor yielded a precise, repeatable response with no apparent elastic hysteresis. The edge behavior of the diaphragms suggests that there is likely no horizontal delamination of the diaphragm layers when pressure is applied. Consistency between prints was lacking; however, each sensor demonstrated precision. The results of this work show that FDM printed parts can be functionally integrated with sensing elements and individually calibrated to produce repeatable readings.

The results presented in this paper support the case for embedded elements in 3D-printed parts as a component of the FDM process cycle. Additionally, the observations that the ABS plastic diaphragm experienced no significant elastic hysteresis or delamination of horizontal layers effectively challenge the negative preconceived notions surrounding printed ABS versus bulk ABS that has caused FDM printing to enter the trough of disillusionment on the economic curve of expectations. The material behavior of the printed ABS is similar to those of a mesoscale, structurally homogeneous diaphragm. This means that it is possible to take advantage of the flexible properties of this material.

This sensor would be well-suited as a demonstration workpiece in either a high-school or college classroom, where it would operate at room temperature only. The design is conducive to teaching students how to design parts for the overhang constraints of a 3D printer. At the same time, it introduces the concepts of in-situ processing, post-processing, and embedded electronics to the FDM process.

Embedding sensing elements into a 3D-printed part can be done safely, quickly and precisely by slightly altering the process to fit the application. Future research may benefit from exploring embedding techniques that are compatible with this bottom-up fabrication process. Furthermore, sensing elements may be embedded into FDM objects without the use of pre-fabricated elements—electroplating ABS cavities with conductive material or screen printing conductive leads may also be promising techniques for embedding sensing elements in FDM objects. Focusing on the development of techniques for embedded circuit boards, conductive leads, and sensing elements may allow the market of FDM printing to push beyond the strictly static model prototyping role it fulfills now.

ACKNOWLEDGEMENTS

This research was supported by National Science Foundation Award ECCS-1542164 which is part of the NSF National Nanotechnology Coordinated Infrastructure (NNCI).

REFERENCES

- [1] Ivan Gajdoš, Jan Slota, "Influence of Printing Conditions on Structure in FDM Prototypes," *Technical Gazette* 20, no. 2 (2013).
- [2] Griselda Saucedo, Douglas Jackson, Kevin Walsh, "3D Printed Piezoresistive Pressure Sensor," IMPACT Research Experience for Undergraduates (October 2016).
- [3] Minquel Domingo-Espin, et al., "Fatigue Performance of ABS Specimens Obtained by Fused Filament Fabrication," *Materials* 11, (December 2018), doi: 10.3390/ma11122521
- [4] Pete Basiliere, Michael Shanler, "Hype Cycle for 3D Printing, 2017," *Gartner Inc.*, (July 2017), https://www.gartner.com/doc/3759564/hype-cycle-d-printing
- [5] Tyler Blumenthal, et al., "Aerosol Jet Printing onto 3D and Flexible Substrates," *Quality in Engineering, Science, & Technology*. OUEST Integrated Inc.
- [6] Gregory Kiesel, et al., "Practical 3D Printing of Antennas and RF Electronics," Advanced Concepts Lab, Georgia Tech Research Institute.
- [7] Shweta Agarwala, et al., "Aerosol Jet Printed Strain Sensor: Simulation Studies Analyzing the Effect of Dimension and Design on Performance," *IEEE Access*, (September 2018), doi: 10.1109/ACCESS.2018.2876647
- [8] 3D Printers Users Guide. Zortrax, (2018)
- [9] M. Samykano, et al., "Mechanical property of FDM printed ABS: influence of printing parameters," *The International Journal of Advanced Manufacturing Technology* 102, (February 2019), doi:10.1007/s00170-019-03313-0
- [10] Karl Hoffman, "Applying the Wheatstone Bridge Circuit," *Hottinger Baldwin Messtechnik GmbH*
- [11] Giovanni, M.D. Flat and Corrugated Diaphragm Design Handbook. New York: Dekker, 1982. ISBN: 0824712811.
- [12] *P3 Strain Indicator and Recorder*. Vishay Precision Group, Document #11102, (May 2011), http://www.vishaypg.com/docs/11102/p3.pdf